Energy & Buildings 298 (2023) 113576

Contents lists available at ScienceDirect

Energy & Buildings

journal homepage: www.elsevier.com/locate/enbuild

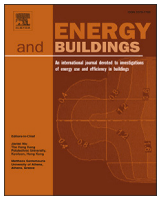

Enhancing self-consumption for decarbonization: An optimization strategy based on a calibrated building energy model

José Eduardo Pachano [a], María Fernández-Vigil Iglesias [a,*], Antonis Peppas [b], Carlos Fernández Bandera [c]

[a] School of Architecture, University of Navarra, 31009 Pamplona, Spain
[b] School of Mining and Metallurgical Engineering, National Technical University of Athens (NTUA), Athens, Greece
[c] Polytechnic School, University of Extremadura, 10003 Cáceres, Spain

ARTICLE INFO

Keywords:
Building energy models (BEM)
HVAC
Internal thermal mass
Variable refrigerant flow (VRF)
EnergyPlus
Set-point optimization

ABSTRACT

To face the challenge of climate change and achieve the decarbonization target set by the European Union, the current trend is to electrify building services, replacing the use of fossil fuels for renewable energy sources. The installation of grid-connected photovoltaic (PV) systems is becoming a popular strategy. However, the widespread application of PV solutions carries certain concerns about grid-network security and stability, since intermittent renewable energy excess pouring into the grid may exceed voltage limits. Therefore, an optimization of the consumption of a building's own PV production (self-consumption) to reduce the excess output is vital. The following paper performs a demand side optimization strategy of the building's thermostatic controllable loads (heating and cooling), which represent at least 50% of the total energy consumed by the building. The process is applied in a previously calibrated building energy model (BEM) that describes a fully operational building under a typical Mediterranean climate (Greece). The site contains a PV plant and a multi-split Variable Refrigerant Flow (VRF) system dedicated to maintain indoor comfort conditions. The technology used is simple, able to perform 15 minute time-step yearly optimizations while saving a large amount of computational time. It performs a bi-dimensional optimization of both: indoor thermal-zone set-points and ventilation air supply temperature. The optimization process performed is based on 2019 data gathered from European Project SABINA, resulting in a self-consumption improvement of 11.6% for summer scenario (reaching 69.16%) and 78.7% for winter (reaching 57.47%) in comparison to a non-optimized "business as usual" base model.

1. Introduction

The European Union's commitment to achieve decarbonization and to reduce greenhouse gas emissions, in order to transition to a carbon-neutral economy, has led to a growing interest in the use of renewable energies and the reduction of fossil fuel dependency.

With the energy strategy established by the European Union (EU) for the coming years and contained in the "Clean Energy for All Europeans" package [1], the aim is to achieve climate neutrality by 2050. To this end, a series of targets are proposed to be achieved by 2030. Among them, it can be highlighted: a commitment to reduce greenhouse gas emissions by at least 55% compared to 1990 levels, ensuring that at least 40% of energy consumption comes from renewable sources, and achieving a minimum energy efficiency improvement of 32.5% [2,3].

Within these objectives, special emphasis is placed on improving the energy performance of the building sector, since it is the largest consumer of energy: buildings account for 36% of greenhouse gas emissions and 40% of final energy consumption in Europe [2], making this sector a critical factor in the decarbonization transition.

The role of photovoltaic energy is crucial in this scenario of carbon dioxide (CO_2) emissions reduction, increase of renewable energies and the growing electrification of several sectors, such as transport, industry or heating and cooling [4]. The aim of this paper is, in line with the route established by the EU, to delve into the possibility of improving the energy performance of a building by optimizing the use of the electrical energy produced in a photovoltaic (PV) plant.

Precisely, matching the local production of renewable energy to the energy demanded by the building is one of the challenges that needs to be met in order to achieve the targets set by the EU. According to Di-

* Corresponding author.
E-mail addresses: jpachano@unav.es (J.E. Pachano), mfernandez-@unav.es (M. Fernández-Vigil Iglesias), cfbandera@unex.es (C. Fernández Bandera).

https://doi.org/10.1016/j.enbuild.2023.113576
Received 13 June 2023; Received in revised form 4 September 2023; Accepted 20 September 2023
Available online 25 September 2023

rective 2010/31/EU [5], amended by Directive (EU) 2018/844 [6], by 2020 all new buildings should be nearly zero-energy buildings (nZEB), that is, buildings with very high energy performance and whose energy needs come from renewable sources.

A net zero energy building (NZEB) connected to the grid uses energy sources such as electricity or natural gas when the on-site generation cannot meet the demand needs. Instead, it exports the excess of renewable energy generation to the grid when that demand is surpassed [7,8]. In other words, the traditional NZEB model uses the grid as an energy excess storage. However, this energy excess is not always an advantage. The intermittent, fluctuating and weather-dependent nature of renewable energies limits the penetration of them in distribution systems [9]. The rapid growth of renewable energy generation capacity can create operational challenges for utilities [10]. In the case of PV generation, it could affect the stability of the electrical system, cause power quality issues, or protection problems. One of the major problems limiting this penetration of PV energy into the grid is the voltage rise caused by the mismatch between production and demand, when the number of connected PV systems is high, and the voltage limit is exceeded in low demand situations [11]. All these reasons make it necessary to establish strategies in order to control these variables and correctly integrate PV systems into the power grid without compromising security and quality of supply [12]. It is necessary the development of different strategies in order to move from the traditional unidirectional to fluctuating bidirectional power flows in the distribution grid.

One of the ways to continue developing PV generation units, a key element in the decarbonization process, is the electrical self-consumption (SC) model, that is, promoting the instantaneous consumption of the energy produced [12]. This solution has started to be used in many countries, such as Germany, Spain and Italy, to prevent an excess of energy overloading the distribution grid [11,13].

Photovoltaic self-consumption has many benefits such as the improvement in the efficiency of the energy system by avoiding transport losses, the reduction of the stress on the electricity distribution grid, a possible reduction of energy prices in the wholesale market, or a reduction in the volume of CO_2 emissions [14–17].

In order to promote self-consumption in residential buildings, there are two different approaches: Demand Side Management (DSM) strategies or energy storage in batteries. There is a lot of literature about the optimization of the batteries, which can present a lot of advantages for the residential PV microgrid systems, but whose costs are currently higher that their benefits [18].

Therefore, this paper is focused on the demand side management approach as a strategy to increase self-consumption. This strategy aims to achieve the energy flexibility, which can be defined as:

The ability to manage its demand and generation according to local climate conditions, user needs, and energy network requirements. Energy Flexibility of buildings will thus allow for demand side management / load control and thereby demand response based on the requirements of the surrounding energy networks [19].

Among the DSM strategies, there are two principal categories: Model Predictive Control (MPC) and rule-based control (RB). The first require more sophisticated algorithms and, particularly, a long run-time for computational simulation. In the present study, a RB strategy to increase self-consumption through the building mass thermal activation is proposed and applied to a real case study through the use of a calibrated building energy model.

MPC strategies are more often present in the literature than RB techniques [20,21]. Some examples of the application of rule-based control strategies can be found in [22], where the authors presented a rule-based strategy for managing the energy resources of a building in the south of France, equipped with a PV plant, a wind turbine and batteries. The strategy is based on the prediction of the grid load, the renewables production and the occupation of the building. Pinamonit et al. [23] developed a simple RB control strategy to manage heating and cooling in a residential building equipped with a heat pump. The strategy consisted of storing the PV surplus in the thermal mass of the building and in two water tanks. They concluded that the thermal capacitance activation was favorable for both winter and summer seasons, and it can increase SC rate in a range from 33% to 40%. In [24] the authors proposed a rule-based control strategy that uses the building thermal capacitance as an energy storage by running the heat pump to its limit when there is a PV production surplus. Thus, the strategy increased the set-point of a water tank and the ambient air temperature. The results showed a significant reduction in the energy exchange between the grid and the building. In the study [25], the building was equipped with a heat pump, which was started by the RB controller when the PV production exceeded the non-heating loads. Results showed that self-consumption could be improved by almost 40%, and the energy bills could be reduced by 19%. However, the price-based control and the self-consumption control display diametrically opposed behaviors to each other. Schibuola et al. [26] studied three different RB heat-pump control strategies, based on the cost of electricity and on the electricity production from the PV plant. The controller was simple: the heat pump (HP) was forced to switch on when prices are low or when the PV panels were generating electricity. Several RB strategies were investigated in [27], applied in the production of domestic hot water for dwellings equipped with heat pumps, and based on voltage measurement.

None of the aforementioned papers applied their proposed strategy to a calibrated model, but to a detailed simulation environment. Also, as it can be appreciated, the most frequent heating, ventilation and air conditioning (HVAC) system optimized in the literature are heat pumps, and it is frequent to find the activation of the thermal mass of the building together with the thermal storage in water tanks.

1.1. Contribution and originality of the research

The original contribution of this research can be summarized in four points, which will be described in detail below:

- The optimization strategy is applied to a calibrated Building Energy Model which fully represents the real thermal behavior of the building.
- The proposed methodology uses a rule-based control strategy, which allows obtaining one year of 15-minute time-step set-points for each thermal zone in a very short computational time.
- Optimization is applied to both the temperature of the thermal zone and the air-supply temperature. Additionally, an analysis of the optimal distribution of the energy surplus was conducted.
- The strategy is executed in multiple HVAC system that provides heating or cooling and ventilation.

This paper presents the application of a novel RB strategy to a real case study, through the use of a calibrated building energy model (BEM). The test site is a two-story building located in Lavrion, Greece. The construction is a living lab from the National Technical University of Athens (NTUA). Unlike most studies that apply demand side management strategies, in this case real data has been used: the BEM has been created, through the calibration of a model using the weather, the PV plant and the HVAC system data collected throughout 2019. All the information about the building was gathered within the framework of the H2020 project “SmArt BI-directional multi eNergy gAteway” (SABINA), funded by the European Commission [28,29]. The main objective of that project was the design of strategies to inject and take advantage of energy excess produced on-site in the building, avoiding exporting it to the grid. The present paper develops one strategy aimed to increase self-consumption for this real building. Therefore, the base model from which the optimization is generated corresponds to the actual operation of the building, respecting the set-points established in the Building Management System (BMS).

The energy consumption has been corrected through the use of a calibrated model: the techniques employed in order to establish the error

of the BEM can be consulted in [30–32]. In [33] and [34] the methodology applied for the calibration of the building envelope was developed. Finally, for the calibration of the HVAC system, the methodology described in [35] and [36] was used.

The DSM strategy was previously successfully tested using synthetic data based on a Building Energy Model (BEM) performed in EnergyPlus. Contrary to the present study, a non-calibrated base model was used, where a perfect knowledge about the PV production, energy consumption and the weather forecast data was assumed [37].

The research applies a rule-based control strategy. These kind of methods work based on algorithms that operate depending on a set of predefined rules to control the system. They are widely used in HVAC systems for temperature control, and they are simple to set up [38]. In this study, the RB technique was used to define, for each room or thermal zone, a set of optimal set-point curves with a fifteen-minute time interval.

Additionally, as it was mentioned before, three issues are analyzed at the same time:

(i) the optimization of the set-point curves of each thermal zone, (ii) the optimization of the set-point curves of the air-supply temperature and (iii) the most appropriate energy distribution in order to achieve that maximum indoor set-points optimization: an energy distribution based on the demand of each thermal zone, a uniform distribution or a distribution based on the air volume.

This evaluation of different practical cases of distributing the energy from the PV and delivering it into the various HVAC systems, establishes new guidelines and shows which is the best way to perform future optimization processes.

After selecting the best energy distribution, the optimization of the set-points resulted in an average increase in self-consumption of 78.7% (from 32.16 to 57.47) in winter and 11.6% (from 61.96 to 69.16) in summer. The increase in self-sufficiency reached 66.5% (from 9.55 to 15.90) in winter and 6.9% (from 36.44 to 38.95) in summer.

It is important to note that the previous research conducted with simulated data [37] delivered more favorable results, with a greater increase in self-consumption. However, the present test makes use of real data from an actual test site gathered during the execution of SABINA project (“SmArt BI-directional multi eNergy gAteway”, [28]) and demonstrates that the methodology works, even when applied to multiple HVAC systems, signalling that the impact of its results may be influenced by the physical characteristics of the building and the capabilities of the PV plant as well.

Finally, the novelties of this paper include the optimization of multiple HVAC systems at the same time. This is performed in a single run for each of the seasons under analysis (winter and summer) which saves abundant computational resources. The main objective of the developed methodology is the reduction of the amount of energy exported to the grid by using the instantaneous production from the PVs, that is, the improvement of self-consumption; and at the same time, avoiding the increase of energy demanded to the grid.

The implementation of the algorithm presented in this study allows the building’s HVAC system to consume excess energy, storing it inside the building spaces as heating or cooling energy while maintaining comfort and indoor health conditions. The technology optimizes the behavior of preexisting equipment, requires minimal sensor deployment, and avoids the need for battery installations, resulting in reduced installation and implementation costs. By developing this optimization algorithm, the PV plant’s performance is enhanced, excess energy deployment into the grid is minimized, and the building’s self-sufficiency is improved with minimal intervention.

The structure of the present paper is established as follows: Section 2 presents the description of the weather, the building and the Heating, Ventilation, and Air Conditioning system, the calibration methodology and the control strategy applied to the current test site. Section 3 discuss the results obtained for this case study, through the comparison between the base and the optimized model. The optimal distribution of the supplied PV production into the building is analyzed, as well as the optimal set-point curves for the air-supply temperature of the air handling unit and for the thermal zones. Finally, Section 4 lists the conclusions obtained from this real test analysis

2. Methodology

As an alternative storage system to batteries, the demand side management strategies could be classified in two groups: hot water tanks and the activation of the building thermal mass. In this research this latter option is explored, using the surplus of PV production. The final goal is to maximize the match between instantaneous local PV production (P) and the building energy demand (L). In order to achieve that, the surplus of the PV production is stored in the thermal mass of the building, by a bi-dimensional modulation of the set-points in each thermal zone and the one regarding the temperature of neutral air supply belonging to the building’s Air Handling Unit (AHU).

For winter scenario, the reference indoor set-point temperature used is 21 °C, which is the lowest allowable value for indoor comfort during heating operation based on SABINA project parameters. The optimization methodology used during this season allows for the room heating set-point to range between its comfort allowable values of 21 °C to 25 °C. For the summer scenario the reference indoor set-point used is 27 °C, the optimization process allows this value to range between its comfort allowable values o 23.5 °C and 27 °C.

Additionally, the reference set-point for the neutral air supply of the AHU dedicated to provide ventilation into the spaces is set to 17 °C for Winter and 30 °C for summer season. The optimization methodology allows the range of this set-points to vary between 17 °C and 24.5 °C during heating operation, and between 23 °C and 30 °C during cooling operation respectively. Since this provides neutral air into the thermal zones that will be further treated by the main VRF system, the main condition of maintaining indoor temperature within comfort values is always observed.

The methodology is applied in a building located in Lavrion, Greece, equipped with a PV system of 15.1 kWp with a 16% efficiency, a PV plant that according to the data used was able to supply a total yearly energy rate of 6575.42 kWh (3783.64 kWh in summer and 2791.78 kWh in winter) under 2019 weather conditions. Additionally, the selected test site building HVAC is comprised of a variable refrigerant flow (VRF) system with a nominal cooling capacity of 71 kW, and 80 kW for Heating.

Next, the characteristics of the weather, the building and the HVAC system are described.

2.1. Weather information

As it was mentioned before, previous work with synthetic data from a dwelling in Pamplona (Spain) was performed [37]. In this case, the proposed algorithm is tested using one year of real data from a PV plant located in Lavrion, Greece. The site is located in a “typical Mediterranean climate”, according to Köppen Climate Classification. It belongs to the category of Hot-Summer Mediterranean Climate (Csa), which is characterized by sunny and dry hot summers with eventual thunderstorms and shower rains and mild winters with a surplus in rain, yet rarely any snow [39].

The present study attempts to perform a 10 minute time-step optimization of the PV plant using the building as a thermal battery for storing the surplus of PV production. The summer operation set up of the equipment involved in this process runs in cooling mode from May 2019 to October 2019, with temperature ranges from 10 °C (Minimum in May) up to 36.6 °C (Maximum in July) and a monthly average horizontal radiation of 441.9 W/m^2, as Table 1 shows.

For its winter operation set up, running from January to April 2019 and from November to December 2019, the HVAC system is shifted and locked into heating mode. Table 2 shows that the site temperatures

Table 1
On-Site summer 2019 operation weather details.

Description		Units	Summer Optimization Period						
			2019						Average
			May	Jun	Jul	Aug	Sep	Oct	
			COOLING						
Outdoor DryBulb Temperature	Average	˚C	19.536	26.208	27.545	28.185	24.243	21.137	24.476
	Maximum	˚C	30.600	34.400	36.600	35.900	30.800	29.400	32.950
	Minimum	˚C	10.000	16.600	19.100	20.400	14.400	13.700	15.700
Global Horizontal Radiation	Average	W/m^2	430.879	488.231	490.833	490.507	424.419	326.207	441.846
Diffuse Radiation	Average	W/m^2	285.090	305.600	294.535	285.452	216.690	141.005	254.729

Table 2
On-Site winter 2019 operation weather details.

Description		Units	Winter Optimization Period						
			2019						Average
			Jan	Feb	Mar	Apr	Nov	Dec	
			HEATING						
Outdoor DryBulb Temperature	Average	˚C	9.923	10.656	13.575	15.176	18.290	13.087	13.451
	Maximum	˚C	17.400	18.100	22.300	25.900	26.900	19.800	21.733
	Minimum	˚C	-0.100	4.300	5.300	6.900	11.200	5.700	5.550
Global Horizontal Radiation	Average	W/m2	118.928	84.686	139.145	205.342	62.785	51.602	110.415
Diffuse Radiation	Average	W/m2	62.785	51.602	120.787	162.467	214.802	271.270	147.286

Table 3
Sensors and accuracy values of the weather station.

Sensor	Units	Range	Resolution	Accuracy
Temperature	˚C	-40˚ to +65˚	±0.1	±0.5
Humidity	%	0 to 100	±1.0	±3.0% (0-90) ±4.0% (90-100)
Global Solar Radiation	W/m^2	0 to 1500	1	≤10
Diffuse Solar Radiation	W/m^2	0 to 1500	1	≤20
Wind Speed	m/s	1 to 67	0.44	±1/±5%
Wind Direction	˚	1 to 360	1.0	±4%
Precipitation	mm	—	0.2	±4%/0.25 (≤50 mm) ±5%/0.25 (≥50 mm)
Atmospheric Pressure	mbar	880 to 1080	±0.1	±1

range from -0.10 ˚C (Minimum in January) to 26.90 ˚C (Maximum in April) with a monthly average horizontal radiation of 110.415 W/m^2.

Since weather directly influences the building's energy demand, stressing its envelope and affecting the performance of HVAC production systems [32,40], it is one of the main aspects to carefully observe in order to perform any building energy strategy [41]. This is particularly evident when analyzing cooling/heating performance of outdoor production units like heat pumps and variable refrigerant flow units. The thermal performance and energy consumption of these equipments are usually directly correlated to weather parameters. For these reasons, a weather station has been allocated on the test site to collect data every fifteen minute time-step. Table 3 displays the station sensors and their accuracy.

Fig. 1. H2SusBuild Test Site's main entrance [36].

2.2. Building description

The test site labeled as H2SusBuild, includes a building that aims to achieve a Net Zero Energy Building (NZEB) status. This building operates as a living lab for the National Technical University of Athens (NTUA), Greece. The building is located inside Lavrion Technological and Cultural Park (LTCP) at an altitude of 26 meters above sea level. As displayed in Fig. 1, the building used for this study is a two-story light construction industrial unit refitted for energy studies purposes. The site is characterized by its little thermal mass, with an envelope consisting of 10 cm expanded polystyrene (EPS) insulation between two layers of lightweight concrete blocks (U value = 0.25 W/m^{2}K). Its roof construction consists of a metallic sandwich panel with a polyurethane insulation layer of 2.5 cm (U value = 0.75 W/m^{2}K) [42].

In order to condition the air volume of the different areas in the building, maintaining their indoor climate and satisfying their comfort constrains, the building employs two Heating, Ventilation, and Air Conditioning (HVAC) systems that operate independently. The first one is a two-way pipe multi-split Variable Refrigerant Flow (VRF) system dedicated to provide both heating or cooling, and ventilation, to the southern side of the structure. The second one, which is outside the

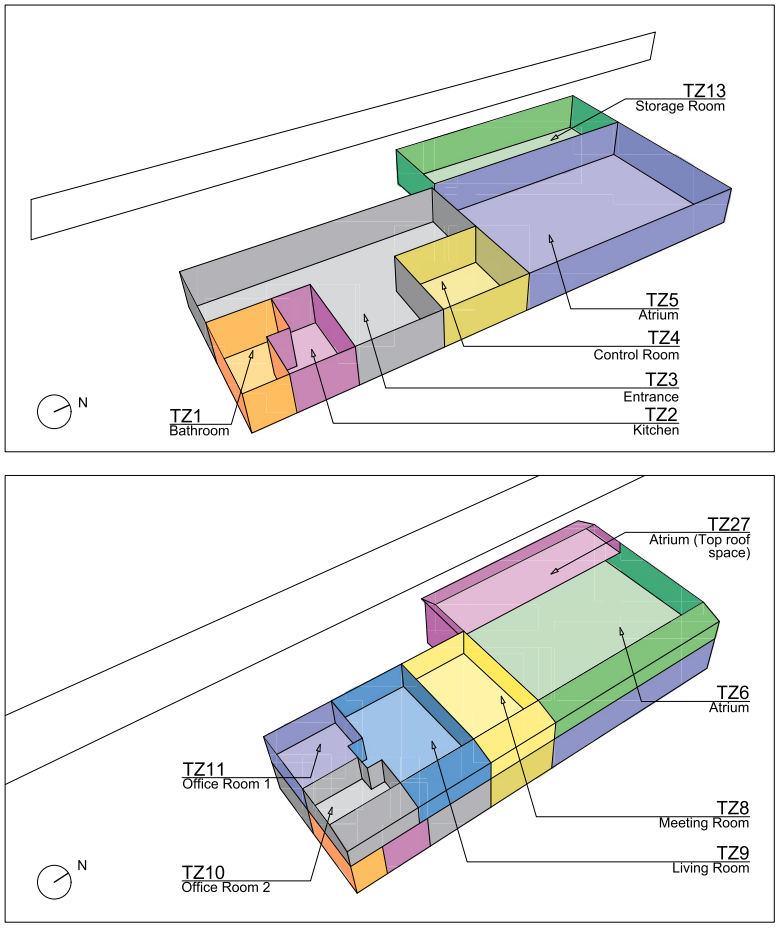

Fig. 2. Building thermal zone: Ground Floor Plan (Top). First Floor Plan (Bottom) [36].

Table 4
Conditioned thermal zone's effective floor area and indoor air volume.

	TZ02	TZ03	TZ04	TZ08	TZ09	TZ10	TZ11	TOTAL
Area (m^2)	13.72	98.39	25.38	50.43	54.44	23.85	23.82	290.03
Volume (m^3)	42.52	305.00	78.66	182.27	160.50	58.39	113.64	940.98

scope of this study, is a Heat Pump (HP) system dedicated to provide heating or cooling, as well as ventilation, to the atrium located on the northern side of the building.

Based on the building technical information, of the total building's air volume of 2475.93 m^3, 420.33 m^3 are set as unconditioned spaces such as storage areas and toilets. Of the remaining conditioned air volume, 1114.62 m^3 are outside the scope of this study since they are part of the atrium served by the HP system. That leaves a total of the 940.98 m^3 of air to be conditioned by the VRF system. The architectural layout displayed on Fig. 2 shows the Thermal Zones (TZ) that are bound to this system and therefore part of this study. Table 4 lists the areas and volumes of each of the following spaces: kitchen (TZ02), main entrance (TZ03), control/server room (TZ04), meeting room (TZ08), living room (TZ-09), and offices (TZ10-11).

In order to minimize the introduction of uncertainty from thermal effects of adjacent TZ that are either unconditioned or outside the scope of this study their indoor behavior is fixed. In the case of unconditioned spaces the indoor temperature values are fixed to the actual room temperature values obtained by sensors deployed in the building; while in the case of the atrium, its indoor temperature values are fixed on the operating set-point schedule requested by the BMS. Thus, the heat transference effects that the atrium and any unconditioned zone has over their adjacent conditioned zones is taken into account inside the model, so the uncertainty that this system may introduce into the BEM is reduced.

2.3. HVAC description

The present study focuses on the variable refrigerant flow HVAC system. The installed equipment is composed of a direct expansion circuit that allows the rate of refrigerant flow to vary depending on the operation of the multiple Electronic Expansion Valves (EEV) inside the room indoor units and the speed of its outdoor unit compressor [43].

As displayed on Fig. 3, the equipment configuration has a tandem outdoor unit with a cooling capacity of 71 kW and a heating capacity of 80 kW designed to operate with an outdoor temperature range from -5 to 43 °C (cooling) and from -20 to 15.5 °C (heating). The outdoor unit is connected to 13 wall mounted VRF Fan Coil Units (FCU) located inside the different TZ and classified based on their cooling/heating capacity as: Type-28 (C 2800 W/ H 3200 W), Type-45 (C 4500 W/ H 5000 W), Type-56 (C 5600 W/ H 6300 W), and Type-71 (C 7100 W/ H 8000 W). Additionally, the outdoor unit is also connected to a direct expansion coil (C 15000 W/ H 10000 W) located inside the auxiliary Air Handling Unit (AHU) that is dedicated to provide ventilation into the aforementioned TZ.

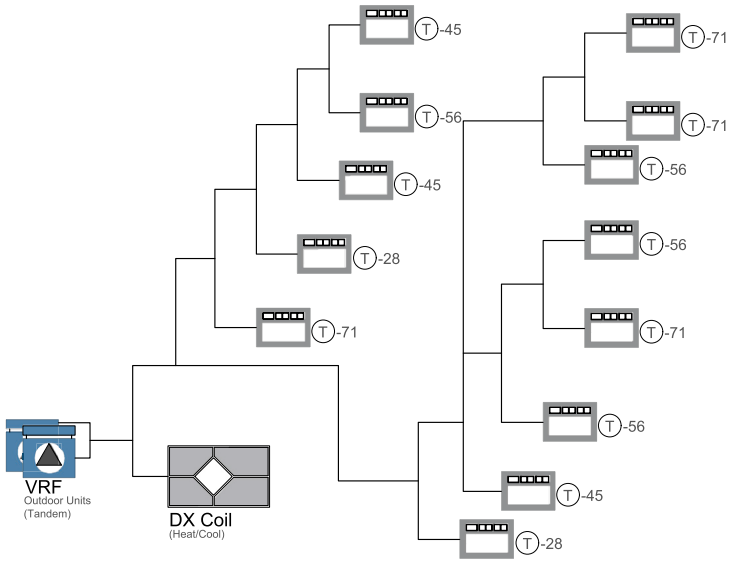

Fig. 3. H2SUS HVAC VRF Installation diagram [36].

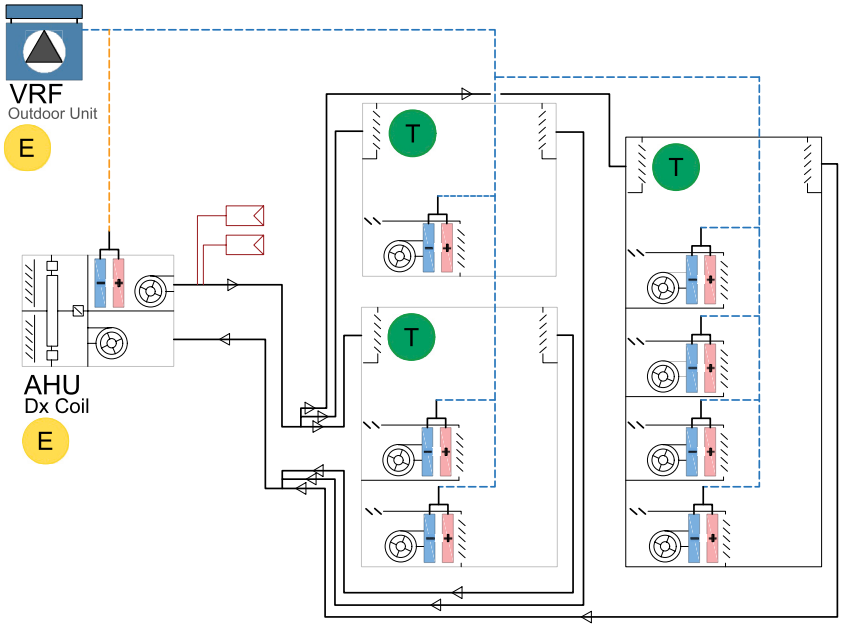

Fig. 4. Overview of H2Sus HVAC VRF Installation diagram [36].

The previously described VRF system operational behavior and electric consumption has a strong relationship between: indoor temperatures and outdoor climate. It functions as a thermal-electric transformer whose operation performance is constrained by the relationship between the building indoor climate and its outside weather conditions. As previously stated in multiple papers by the authors [44,36], the effects produced by the building's internal loads (occupancy, lighting and equipment) are represented in the actual indoor temperatures of the multiple thermal zones within the building. The BEM calibration process is performed in two steps, where its envelope calibration is executed during free oscillation periods and thus there is no effect from the buildings internal loads. However, it is to be noted that during the building's HVAC system calibration, the BEM's resulting indoor temperatures are continuously benchmark against actual readings by the use of uncertainty indexes. Therefore the effects produced by these internal loads are introduced into the obtained HVAC calibrated parameter values.

2.4. Calibrated building energy model description

The building and its HVAC installation is modelled in detail in DesignBuilderV6 software, generating a baseline model that is exported into EnergyPlus simulation environment. The main criteria used to generate this model are to simulate the building and its components in a way that they resemble real conditions as closely as possible, introducing into the model as much information for the constructions and equipment as available in the technical documentation. As Fig. 4 shows, it is here that the building TZ are geometrically set, the nodes for the HVAC equipment are introduced and their loops described, setting all parameters to technical specifications.

After the baseline model has been generated, its envelope undergoes calibration using the methodology stated by Ramos et al. [33], and validated by Gutierrez et al. [45], and its HVAC system parameter values and performance curves have been calibrated and validated by

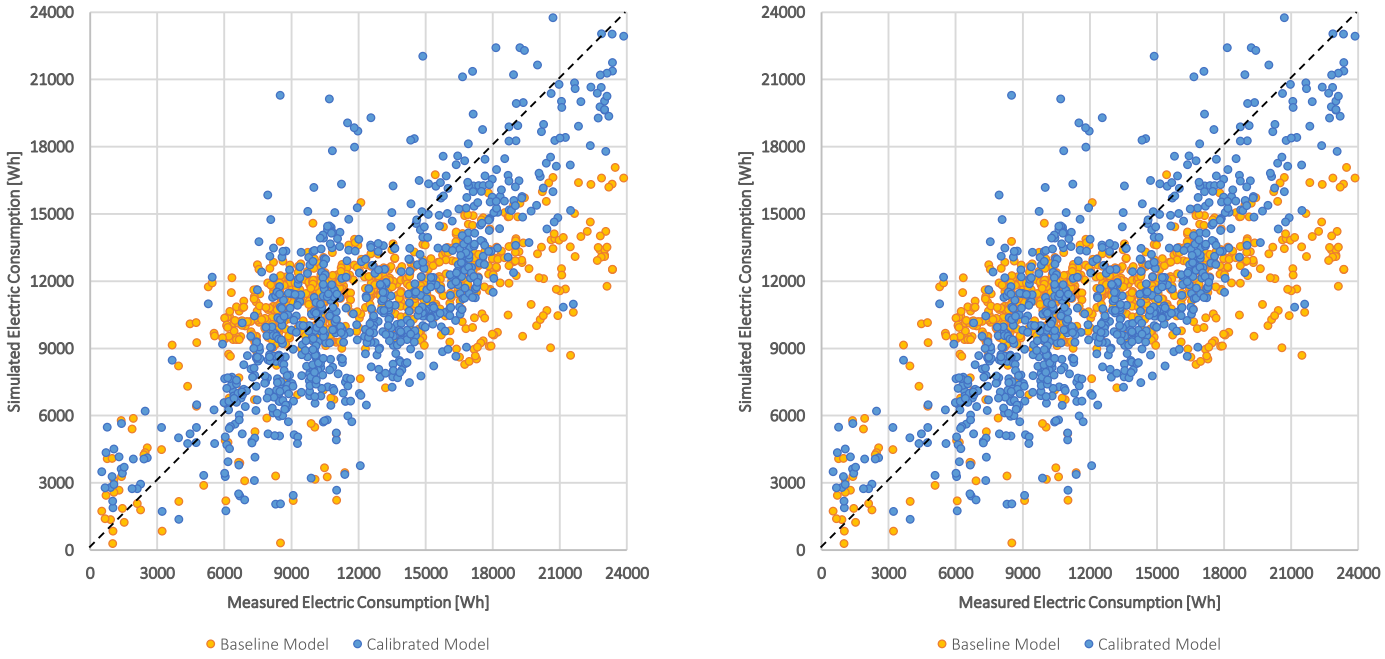

Fig. 5. Performance results for electric consumption of the calibrated BEM for Heating (left) and Cooling (right). (For interpretation of the colors in the figure(s), the reader is referred to the web version of this article.)

Table 5
Electric Consumption hourly uncertainty index for the BEM Calibration period.

	International Standard		Electric Consumption Results	
INDEX	ASHRAE	IMPVP	Heating Calibration	Cooling Calibration
NMBE	±10%	±5%	10.234%	7.139%
Cv(RMSE)	30%	20%	27.180%	25.681%
R^2[a]	75%	75%	59.473%	75.300%

[a] Although there is no universal standard for a minimum acceptable R^2 threshold, values above 75% are often considered a sign of a good causal relationship amongst the energy and independent variables [46].

Pachano et al. [36]. Therefore, the current study is performed on a fully calibrated Building Energy Model (BEM).

2.5. Calibrated building energy model results

The calibrated parameter values and curves obtained allowed the BEM to capture the building thermal behavior and match its energy consumption. As Fig. 5 shows, the simulated values for electric energy cluster around the ideal 45° line for both Heating and Cooling.

In regard of the quality of the performed calibration, Table 5 displays the electric consumption uncertainty indexes obtained after the calibration process has ended. The resulting calibrated BEM model seems to comply with ASHRAE's standard.

In terms of indoor temperatures, the calibrated BEM capture the thermal behavior of the different spaces with a good correlation. Keeping all temperature uncertainty indexes below the requirements suggested by Chartered Institution of Building Services Engineers (CIBSE) on its publication Operation Performance TM-63. Moreover, not one of such temperature errors is above 1 °C. Table 6 shows the indoor temperature indexes for Heating calibration, while Table 7 displays those for Cooling calibration.

The results obtained from these calibrated BEM models show that the energy model has truly captured the indoor climate behavior of the building, and the consumption of its equipment. Therefore, the calibrated BEM models faithfully represent the working conditions of the building and can now be used for the following PV optimization process.

2.6. Control strategy

Fig. 6 describes the process used in order to obtain the optimal set-points curves. For the base case, real data was collected during one year, 2019. The simulation of the base scenario was performed with fixed temperatures using the reference set-points in the thermal zones of: 27 °C in summer and 21 °C in winter. As it was mentioned before, in addition to the Fan Coil Units, the VRF outdoor unit is connected to an auxiliary AHU. Its air supply temperature set-point was fixed at 30 °C in summer and 17 °C in winter.

This first simulation allows to obtain the Coefficient of Performance (COP) of each step-time and the distribution of the energy excess within the different thermal zones.

The second step consisted of obtaining the optimal set-points, based on the files collected in the first stage. When the demand of the building was higher than the energy produced by the PV plant, the standard set-points were applied. By contrast, when there was an excess PV production, the optimal temperature subroutine was executed in EnergyPlus Runtime Language (Erl).

Nine different optimized models were simulated, obtained by the combination of two factors. On the one hand, the defined algorithm distributed the excess of energy into the TZ according to three different approaches: the distribution results obtained in the first simulation, that is, the calibrated distribution; a distribution based on the floor area of each TZ, and a distribution based on the air volume of each TZ. On the other hand, three different priority approaches were tested: first, the excess of energy was distributed to the VRF and the AHU simultaneously, secondly the excess of energy was prioritized to be distributed to the

Table 6
Indoor thermal zone temperature hourly uncertainty index for the Heating Calibration period.

	Indoor Temperature by TZ							Building
INDEX	Tz-02	Tz-03	Tz-04	Tz-08	Tz-09	Tz-10	Tz-11	Average
MAE (°C)	0.170	0.056	0.036	0.375	0.256	0.262	0.397	0.194
RMSE (°C)	0.705	0.198	0.099	0.931	0.763	0.688	0.966	0.462
NMBE (%)	0.699	-0.087	-0.030	1.462	0.980	0.827	1.558	0.712
Cv(RMSE) (%)	3.150	0.968	0.410	4.109	3.171	3.084	4.413	2.086
R^2 (%)	89.474	99.056	99.715	86.797	91.013	82.361	73.875	93.966

Table 7
Indoor thermal zone temperature hourly uncertainty index for the Cooling Calibration period.

	Indoor Temperature by TZ							Building
INDEX	Tz-02	Tz-03	Tz-04	Tz-08	Tz-09	Tz-10	Tz-11	Average
MAE (°C)	0.235	0.054	0.024	0.057	0.138	0.221	0.328	0.100
RMSE (°C)	0.389	0.195	0.046	0.173	0.394	0.619	0.654	0.194
NMBE (%)	-0.584	0.000	-0.004	0.153	0.538	-0.410	-0.810	-0.014
Cv(RMSE) (%)	1.825	0.934	0.189	0.723	1.626	2.844	3.030	0.863
R^2 (%)	93.253	95.819	99.803	98.762	95.021	83.565	73.754	96.759

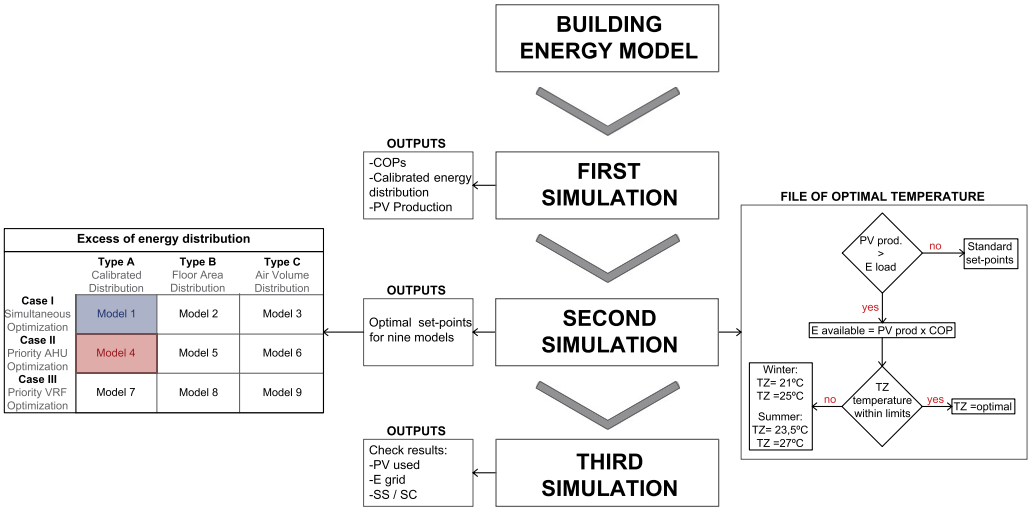

Fig. 6. Control Strategy used in the optimization process, describing the different scenarios under which the study was performed.

AHU, and finally the excess of energy was prioritized to be delivered to the VRF.

The EnergyPlus' object called "OtherEquipment" was run for the nine energy distributions within the different TZ. This object is used in order to introduce sensible heating or cooling into a thermal zone without defining an HVAC system. At this point, the VRF system was OFF. The excess energy for the AHU, which is kept on, is calculated using the Equation (1):

$$E = m * Cp * \delta T, \tag{1}$$

When the excess of energy introduced caused the room temperature to be outside the minimum or maximum comfort allowable limits previously mentioned in Section 2, the algorithm set the thermostat at its minimum or maximum allowable limit values of 21 °C or 25 °C respectively for heating and 23,5 °C or 27 °C respectively for cooling.

In a similar way, when the excess energy provided into the AHU caused its supply air temperature to be outside the limits previously set by the project, the algorithm set the supply air thermostat at its minimum or maximum range. In this case, the limits used are 17 °C or 24.5 °C for heating and 23 °C or 30 °C respectively for cooling operation.

The results of the nine optimized models were analyzed in order to find out which was the optimal energy distribution.

Finally, the third step allowed to check the results. The methodology works correctly when the following items are met:

- The set-points of each thermal zone vary between 21 and 25 degrees in winter and between 23,5 and 27 degrees in summer when there is photovoltaic production. Therefore, the PV energy consumption should be higher in the optimized model than in the base case, and the amount of energy exported to the grid is reduced.
- The AHU supply air set-points vary between 17 and 24,5 degrees in winter and between 23 and 30 degrees in summer when there is photovoltaic production. The fact that this air is further treated by the VRF system deployed in each thermal zone allows to maintain indoor comfort conditions at all times.
- Self-sufficiency (SS) and Self-Consumption (SC) should be higher in the optimized scenario since the methodology aims to maximize the consumption of instantaneous PV energy produced.
- The energy consumed from the grid does not vary more than ± 0,5%. If the optimized model consumes more than 0,5% than the base model, the results are discarded.

The reason behind choosing such a restrictive limit value for the difference of energy consumption (± 0,5%) is based on three main considerations:

First, this limit value is intended to keep all of the models within the same grid consumption range, which allows for a fair assessment of the implications of the optimization methodology currently applied. Moreover, keeping the optimized models within the same grid consumption range allows the evaluation of multiple optimization strategies and at the same time improves the understanding of the building characteristics and behavior under such dynamic scenarios.

Second, by keeping the grid consumption of the optimized model as closely as possible to the obtained in the baseline scenario, the optimization process main focus is set to maximize the consumption of excess PV energy while avoiding an increment on grid consumption. Thus, the results obtained minimize any possible economic affectation regarding the overuse of energy that may be subject to tariffs or bills.

Finally, by keeping this strict margin of comparison we expect the models to minimize any error in the prediction of results obtained after the optimization process has finalized. The margin of 0,5% is expected to be restrictive enough in order to minimize the deviation that would be produced when the methodology is implemented in a future practical approach.

2.7. Energy matching chart

Two grid indicators are used along this paper. They are self-consumption and self-sufficiency, represented in the following equations:

$$\gamma_{sc} = \frac{\int_{t_1}^{t_2} M(t)\,dt}{\int_{t_1}^{t_2} P(t)\,dt} \tag{2}$$

$$\gamma_{ss} = \frac{\int_{t_1}^{t_2} M(t)\,dt}{\int_{t_1}^{t_2} L(t)\,dt} \tag{3}$$

where:
$P(t)$ = Instantaneous on site PV generation;
$L(t)$ = Instantaneous building power consumption;
$M(t)$ = Instantaneous overlapping of generation and load profile;
$M(t) = \min\{L(t), P(t)\}$;
γ_{sc} = Self-Consumption; and
γ_{ss} = Self-Sufficiency.

Self-consumption could be defined as the ratio of the amount of PV production used in the building to the total PV production. Self-sufficiency is defined as the ratio of locally used PV to the total energy consumption of the building.

In order to evaluate the changes that the proposed algorithm produces in self-consumption, the energy matching chart is used. It was firstly developed by Luthander et al. [47], and previous work of the authors added extra information, the color bubbles [37].

As it is shown in Fig. 7 self-consumption and self-sufficiency are represented in a coordinate axis.

The relation between these two concepts is explained in equation (4):

$$\frac{\gamma_{ss}}{\gamma_{sc}} = \frac{P}{L} \tag{4}$$

In the diagram, the red dotted line divides the space in two: net producers above, when self-consumption is lower than self-sufficiency. That means, according to equation (4), that PV production is higher than demand. On the other hand, net consumers are represented below the line, self-consumption is higher than self-sufficiency. Or, in other words, the energy demand of the building is higher than its PV production.

When self-consumption and self-sufficiency are the same, the bubble is positioned in the green dotted line. That is the case of NZEB buildings, when PV production and demand are coincident, P/L = 1. When there is a perfect match between both, the bubble is positioned in the upper corner (SC = 100, SS = 100).

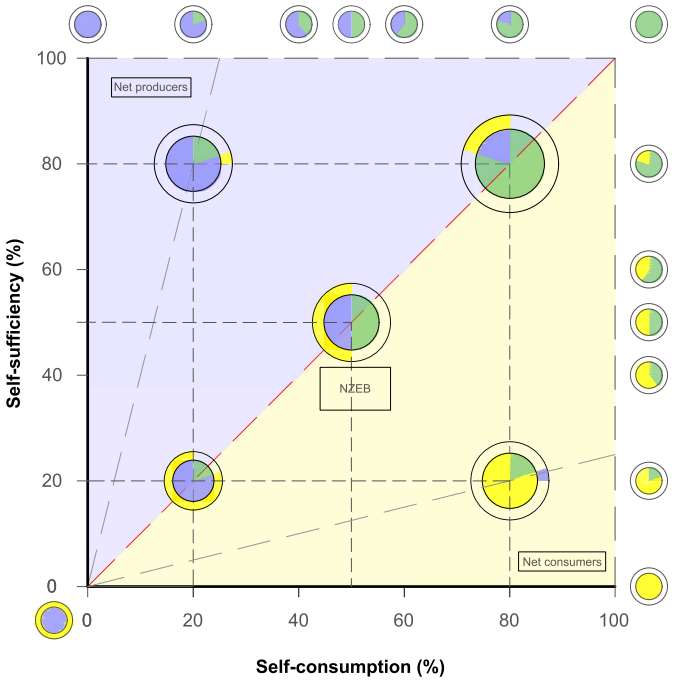

Fig. 7. Color bubbles in the energy matching chart, methodology developed in [37].

With regard to color bubbles, they are a great source of information. Firstly, the size of the bubble is related to L. In addition, the area of the concentric circles is the same, yellow represents demand and blue represents PV production. For net consumers, yellow is represented inside and blue in the ring, and the opposite for net producers. The match between both is the green area inside the circle. In the ring appears the percentage of demand that is not matching the PV production (for net producers), or the percentage of PV production that is not matching the energy demand (for net consumers). More details can be consulted in [37].

3. Results

As it was explained in Section 2.6, nine optimized models were simulated, with different energy distribution approaches. The first letter that labels the optimization cases refers to the process performed; Case I is defined as the simultaneous optimization of both systems (AHU and VRF), Case II refers to the one where the AHU is prioritized, and Case III is based on VRF prioritization over the AHU. The second set of letters that defines the cases (A, B and C) refers to the energy distribution scheme used, these being: a distribution based on calibrated results, by building floor area or by air volume respectively.

The comparison between these models allows to choose the optimal one for both heating and cooling. As it is shown in Table 8, the selected option for cooling was the one based on the calibrated distribution of the energy excess, that feeds simultaneously the AHU and the FCUs. However, in the heating case (Table 9), the model whose excess of energy is distributed based on the calibration results and that feeds first the AHU produced slightly better results.

Those models that produced a grid energy consumption higher than 0,5% with respect to the base model were discarded. Among the remaining, the optimal was the model that had the highest increase in Self-Sufficiency and Self-Consumption, and therefore, a higher percentage of PV energy used.

A general overview of the optimal models' results can be observed in Tables 10 and 11. From May to October, the model is working in the cooling scenario, and the rest of the year, that is from November to April, it is working in the heating scenario.

Table 8
Results Obtained from the multiple optimization cases performed for the yearly cooling scenario (May to October). Any case which does not produce a grid energy consumption similar (±0.50% on Grid Energy Savings) to the baseline model is discarded.

Opt. CASE	PV Produced (kWh)	Energy Consumption [kWh]	PV Used [kWh]	PV Excess [kWh]	Grid Energy Consumption [kWh]	PV Self Sufficiency [%]	PV Self Consumption [%]	Grid Energy Savings [%]
Baseline	3783.64	6433.51	2344.37	1439.27	4089.14	36.44%	61.96%	0.00%
I - A	3783.64	6718.99	2616.96	1166.69	4102.03	38.95%	69.16%	-0.32%
I - B	3783.64	6699.69	2583.72	1199.92	4115.97	38.56%	68.29%	-0.66%
I - C	3783.64	6696.51	2594.32	1189.32	4102.19	38.74%	68.57%	-0.32%
II - A	3783.64	6699.75	2591.27	1192.38	4108.48	38.68%	68.49%	-0.47%
II - B	3783.64	6698.32	2588.28	1195.36	4110.04	38.64%	68.41%	-0.51%
II - C	3783.64	6716.59	2609.78	1173.86	4106.81	38.86%	68.98%	-0.43%
III - A	3783.64	6720.44	2611.46	1172.18	4108.98	38.86%	69.02%	-0.49%
III - B	3783.64	6713.88	2588.94	1194.70	4124.94	38.56%	68.42%	-0.88%
III - C	3783.64	6736.57	2619.53	1164.11	4117.03	38.89%	69.23%	-0.68%

Table 9
Results Obtained from the multiple optimization cases performed for the yearly heating scenario (January to April, and November and December). It is to be noted that any case which does not produce a grid energy consumption similar (±0.50% on Grid Energy Savings) to the baseline model is discarded.

Opt. CASE	PV Produced (kWh)	Energy Consumption [kWh]	PV Used [kWh]	PV Excess [kWh]	Grid Energy Consumption [kWh]	PV Self Sufficiency [%]	PV Self Consumption [%]	Grid Energy Savings [%]
Baseline	2791.78	9399.19	897.91	1893.87	8501.28	9.55%	32.16%	0.00%
I - A	2791.78	10025.54	1524.05	1267.73	8501.50	15.20%	54.59%	0.00%
I - B	2791.78	9942.17	1461.29	1330.49	8480.89	14.70%	52.34%	0.24%
I - C	2791.78	9978.38	1499.09	1292.69	8479.28	15.02%	53.70%	0.26%
II - A	2791.78	10092.02	1604.36	1187.42	8487.66	15.90%	57.47%	0.16%
II - B	2791.78	10071.57	1580.05	1211.73	8491.52	15.69%	56.60%	0.11%
II - C	2791.78	10080.40	1589.42	1202.36	8490.98	15.77%	56.93%	0.12%
III - A	2791.78	10017.99	1317.66	1474.12	8700.33	13.15%	47.20%	-2.34%
III - B	2791.78	9983.79	1302.03	1489.75	8681.76	13.04%	46.64%	-2.12%
III - C	2791.78	10035.45	1349.45	1442.33	8686.00	13.45%	48.34%	-2.17%

Table 10
Monthly evaluation of PV Used and Self-Consumption of the PV plant for both the baseline model and the best optimization case for the yearly heating and cooling scenarios.

Month	PV Produced (kWh)	PV Used (kWh)	PV Used Opt. (kWh)	Increase PV used (%)	SC Base (%)	SC Opt. (%)
January	246.03	182.51	209.52	14.80%	74.18%	85.16%
February	434.91	266.28	359.57	35.03%	61.23%	82.68%
March	900.74	230.93	517.35	124.03%	25.64%	57.44%
April	745.18	108.65	323.51	197.74%	14.58%	43.41%
November	241.91	6.76	41.85	519.36%	2.79%	17.30%
December	223.02	102.78	152.56	48.44%	46.08%	68.41%
Total Heating	**2791.78**	**897.91**	**1604.36**	78.68%	**32.16%**	**57.47%**
May	697.80	228.60	368.73	61.30%	32.76%	52.84%
June	595.22	458.80	465.85	1.54%	77.08%	78.26%
July	732.13	595.46	597.53	0.35%	81.33%	81.61%
August	795.19	634.61	637.38	0.44%	79.81%	80.15%
September	452.03	280.37	295.91	5.54%	62.02%	65.46%
October	511.27	146.53	251.57	71.68%	28.66%	49.20%
Total Cooling	**3783.64**	**2344.37**	**2616.96**	11.63%	**61.96%**	**69.16%**

Tables 10 and 11 show that better results were obtained for the winter months than for the summer ones, with the exception of May and October, for both SC and SS. The PV use increased in an average of 78.7% in winter and of 11.6% in summer. The self-sufficiency increased an average of 66.5% in winter and an average of 6.9% in summer. The self-consumption increase was 78.7% for heating and 11.6% for cooling.

It is interesting to note that, as it happened when this methodology was applied to synthetic data in an apartment building in the north of Spain [37], the increase obtained for self-consumption can be compared with results obtained by using batteries. In [47], the authors compiled several studies that addressed different strategies to increase SC. Although it is not possible to make direct comparisons, since each case depends on various factors such as the climate, the type of building, its constructive characteristics, difference in internal loads due to occupancy and equipment, the energy consumption or the PV production, the results obtained with this methodology demonstrate higher increases than other DSM strategies, which usually increased SC and SS less than 10% [47].

The energy matching chart of every month of 2019 is represented in Fig. 8. In this image is easy to perceive the different behavior that the strategy demonstrates along the year. During the warmest summer months, June, July and August, the methodology only provoke slightly increases in both self-sufficiency and self-consumption. The reason behind this situation is that in all these months the demand is much higher than the production of photovoltaic energy, and already the base model has self-consumption levels above 75%. The optimization of the set-points cannot improve this level of self-consumption much more.

Table 11
Monthly evaluation of Grid Energy Used and Self-Sufficiency of the Building for both the baseline model and the best optimization case for the yearly heating and cooling scenarios.

Month	Demand (kWh)	Demand Opt. (kWh)	Energy Grid (kWh)	Energy Grid Opt. (kWh)	Grid Saving (%)	SS Base (%)	SS Opt. (%)
January	3146.14	3171.45	2963.63	2961.93	-0.06%	5.80%	6.61%
February	2582.28	2671.01	2316.00	2311.44	-0.20%	10.31%	13.46%
March	1281.18	1554.88	1050.25	1037.53	-1.21%	18.03%	33.27%
April	563.26	780.11	454.61	456.61	0.44%	19.29%	41.47%
November	192.07	233.42	185.32	191.57	3.37%	3.52%	17.93%
December	1634.25	1681.14	1531.47	1528.59	-0.19%	6.29%	9.07%
Total Heating	**9399.19**	**10092.02**	**8501.28**	**8487.66**	**-0.16%**	**9.55%**	**15.90%**
May	342.55	483.01	113.95	114.28	0.29%	66.73%	76.34%
June	1427.45	1437.33	968.65	971.48	0.29%	32.14%	32.41%
July	1748.58	1752.44	1153.12	1154.92	0.16%	34.05%	34.10%
August	1801.71	1804.96	1167.11	1167.59	0.04%	35.22%	35.31%
September	793.50	816.05	513.13	520.14	1.37%	35.33%	36.26%
October	319.72	425.19	173.19	173.63	0.25%	45.83%	59.17%
Total Cooling	**6433.51**	**6718.99**	**4089.14**	**4102.03**	**0.32%**	**36.44%**	**38.95%**

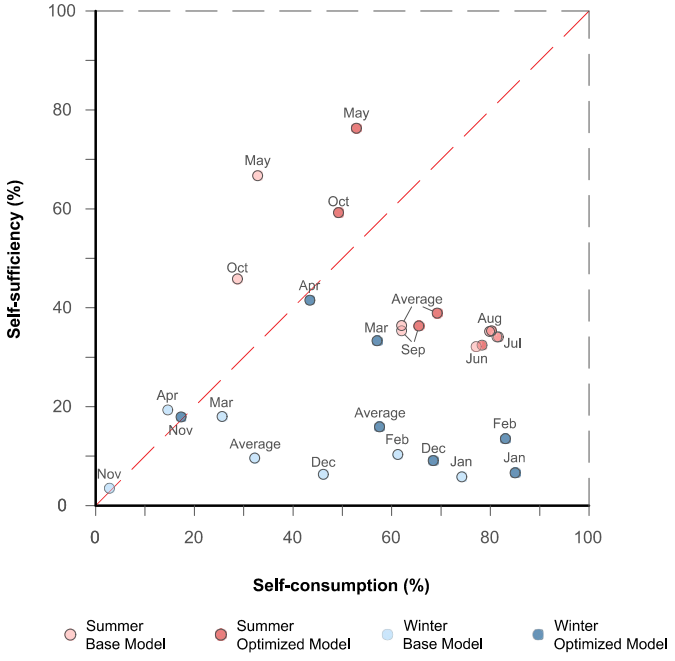

Fig. 8. Monthly baseline versus optimization results in terms of Self-Consumption and Self-Sufficiency.

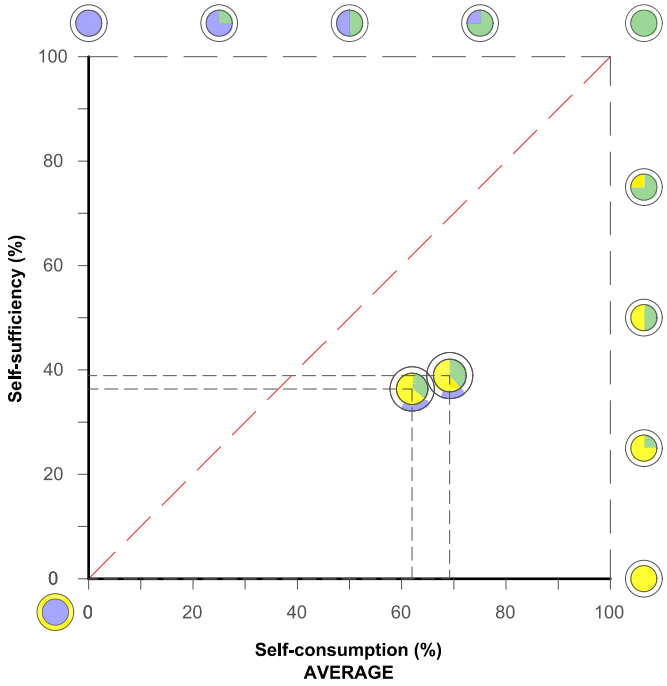

Fig. 9. Summer baseline versus optimization results energy matching chart. (Cooling).

Fig. 9 and Fig. 10 show the energy matching chart for the average results of the base and optimized model for cooling and heating respectively. The color bubbles add some extra information, as it was explained before. The size of the circles is related to the total energy consumed by the building, while the colors represent the matching between PV production and PV used.

In winter, the energy demand is higher, therefore the bubbles are larger than the summer ones. Also, in both cases, the size of the optimized bubbles is slightly larger than the base one. This is due to the over-consumption produced by the strategy when extra PV energy is available. However, this has no impact in the total amount of energy consumed from the grid.

Fig. 11 collects the bubbles for the base and optimized models of every month of 2019. The size of the circles corresponding to April, May, November and October was enlarged 4 times, in order to make them easier to visualize. The reason for this is that, as explained above, the size of the bubbles is proportional to the building energy demand. During these four months the power consumption was very low, so the bubbles were too small and they have been modified to improve their readability.

The green area of these figures graphically represents the matching capacity of each scenario. For those cases that are net-consumers, the green area corresponds to self-sufficiency, the relation between the PV energy used and the demand. On the contrary, when the building is behaving as net-producer (May, October and the base model of April), the green area represents self-consumption. The yellow area is the demand that is not covered by the PVs while the blue area represents the PV production that is not being used. The optimization strategy increases the green area in summer and in winter, as it can be appreciated in Figs. 9 and 10.

3.1. Temperature modulation

As it was mentioned before, the main objective of the developed methodology is the reduction of the amount of energy exported to the grid, by using the instantaneous production from the PVs. At the same time, one requirement of the strategy was to increase self-consumption without increasing the energy demanded to the grid. The way to achieve this is through the modulation of the set-points of each thermal zone

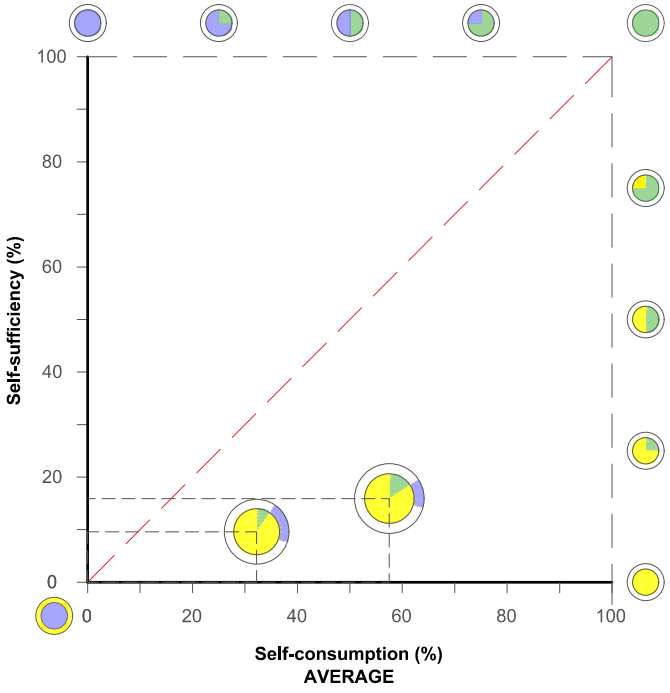

Fig. 10. Winter baseline versus optimization results energy matching chart. (Heating).

within its comfort allowable limits, from 21 °C to 25 °C in winter and from 23,5 °C to 27 °C in summer. To show the impact of the optimization regarding the indoor climate of the building, thermal zone 3 was selected. This TZ corresponds to one of the main areas of the building. Figs. 12 and 13 show the comparison between the baseline fixed set-point and the ones obtained from the optimization process in winter (March 04 to 17) and summer (July 15 to 28) scenarios respectively.

As it can be observed, the fifteen-minute average temperature is represented for each day of the month in both figures. In both cases the obtained indoor temperatures are set between comfort temperature ranges during the operation hours of the building.

For the winter scenario, in the base model the set-point is fixed at 21 °C when the building is operative, while in the optimized model, the set-points varies between the established range of temperatures, reaching the optimal one according to the instantaneous photovoltaic production. When there is an excess of this production, the set-point is fixed at the maximum of 25 °C.

Fig. 13 shows the temperature's behavior in TZ03 during a summer month: August. In this case, when extra energy from the PV panels is available, the set-points of the thermal zone are modified from the fixed 27 °C, to the optimal one within the range from 23,5 °C to 27 °C.

It is important to highlight that in both figures, only the temperature of one specific TZ is represented. However, the fifteen-minute optimal temperature was obtained with the RB strategy for each thermal zone and the optimization was performed for the whole year on a 15 minute time-step, that means a remarkable number of points calculated in a short period of time.

Additionally to the modulation of the TZ set-points, the strategy allows the BMS to modify the air-supply temperature in the AHU. In the base model, this set-point was fixed at 30 °C for summer and 17 °C for winter. In the heating optimized model, as it is shown in Fig. 14, this temperature ranges between 17 and 24,5 °C. For the cooling scenario (Fig. 15), the optimal temperature varies between 23 and 30 °C.

4. Conclusions

Improving the self-consumption of photovoltaic plants is a key element in the transition to a decarbonized world, as it would allow a more extensive and efficient use of renewable energies. The present research analyzes the behavior of a Demand Side Management strategy in order to increase PV self-consumption and, therefore, to reduce the energy dispatched to the grid, which causes important operational problems.

The methodology was applied to a real case, through the use of a calibrated Building Energy Model of a living-lab building located in Greece, using data collected during 2019, within the framework of the European Project SABINA.

The Rule-Based control strategy allows to obtain the optimal set-point for seven thermal zones during one year at each fifteen-minute time-step. Additionally, the optimal option to distribute the excess of PV production into the thermal zones is analyzed. For this reason, nine optimized models were simulated. It was demonstrated that the energy distribution based on the calibration results provided the best optimiza-

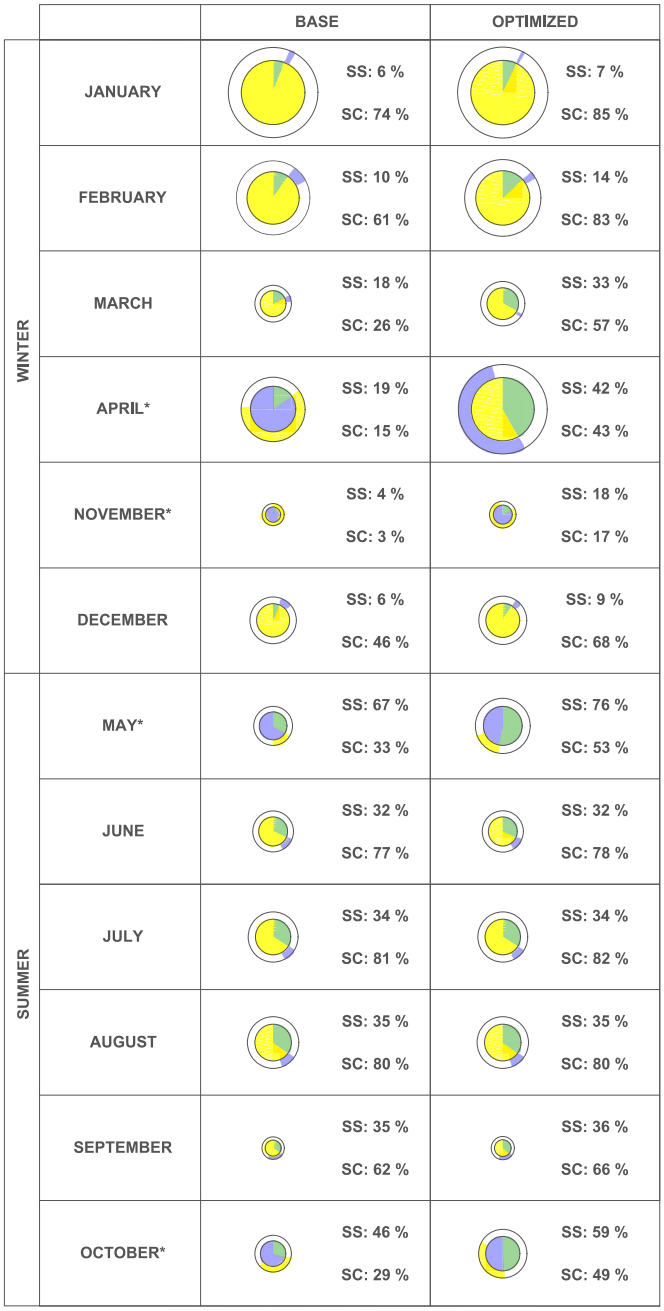

Fig. 11. Monthly baseline versus optimization results using energy matching charts. Note: * indicates that the bubble size was enlarged to improve its readability.

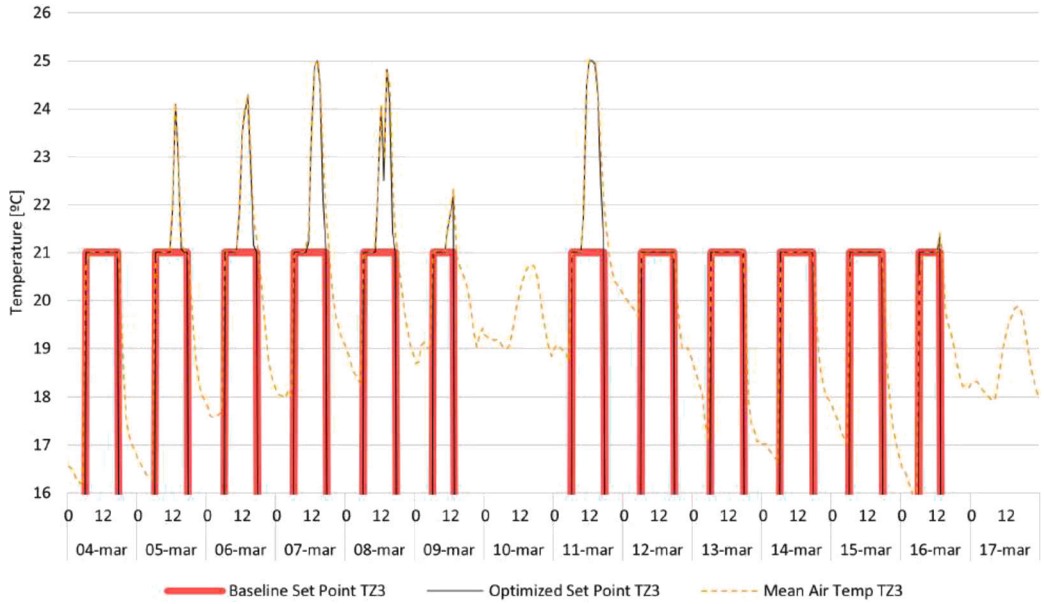

Fig. 12. Thermal zone 3 Indoor Temperature Set-Point comparison between baseline and optimization for March (winter scenario).

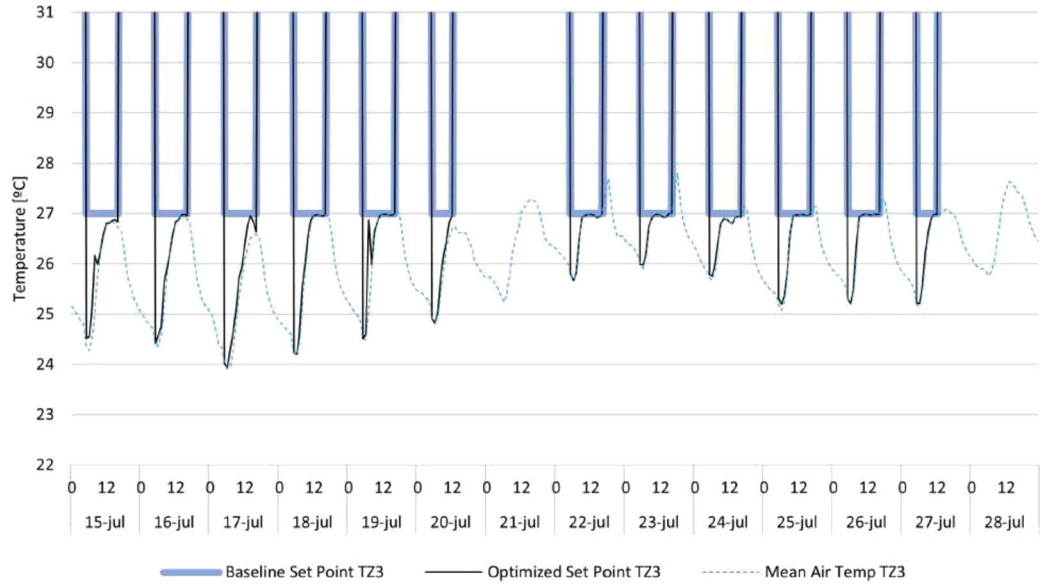

Fig. 13. Thermal zone 3 Indoor Temperature Set-Point comparison between baseline and optimization for August (summer scenario).

tion for both heating and cooling scenarios, being closely followed by the air volume distribution case. Attending to the HVAC systems, the best result in summer was obtained when the AHU and the VRF systems were fed with the extra-energy simultaneously. On the other hand, in winter the optimal model was the one that fed the AHU primarily.

Even though the constructive characteristics of the building are not the most favorable to be used as a thermal inertia storage, the strategy produced quite remarkable results. The average increase of self-consumption during summer reached 11.6 percentage points, while in winter the optimization of the set-points the self-consumption was enhanced by 78.7%. With regard to self-sufficiency, this parameter was increased by 66.5% in winter and by 6.9% in summer.

This approach signifies a promising step toward sustainable energy practices. While larger industrial scenarios may benefit from advanced control algorithms to optimize energy utilization and efficiency, simpler control strategies are sufficient for smaller-scale applications like the residential sector, bolstering future electrification processes while optimizing energy consumption.

The results were explained through the colored bubbles in the energy matching chart, a very useful tool in order to present a lot of outputs at the same time: Self-consumption and self-sufficiency, the matched and unmatched energy produced and used, as well as the amount of energy demanded. When the results are compared with similar studies, it can be appreciated that the present methodology provided better results that similar DSM strategies.

Future works on this study would encompass possible changes in the indoor areas of the building (i.e. increasing the thermal mass of the thermal zones). Additionally, the application of this optimization methodology will be studied in the sizing of the PV plant for both summer and winter scenarios. Last but not least, this process could be applied using weather forecasts and its results introduced into the building, obtaining a comparison between simulated results and the real impact in the building.

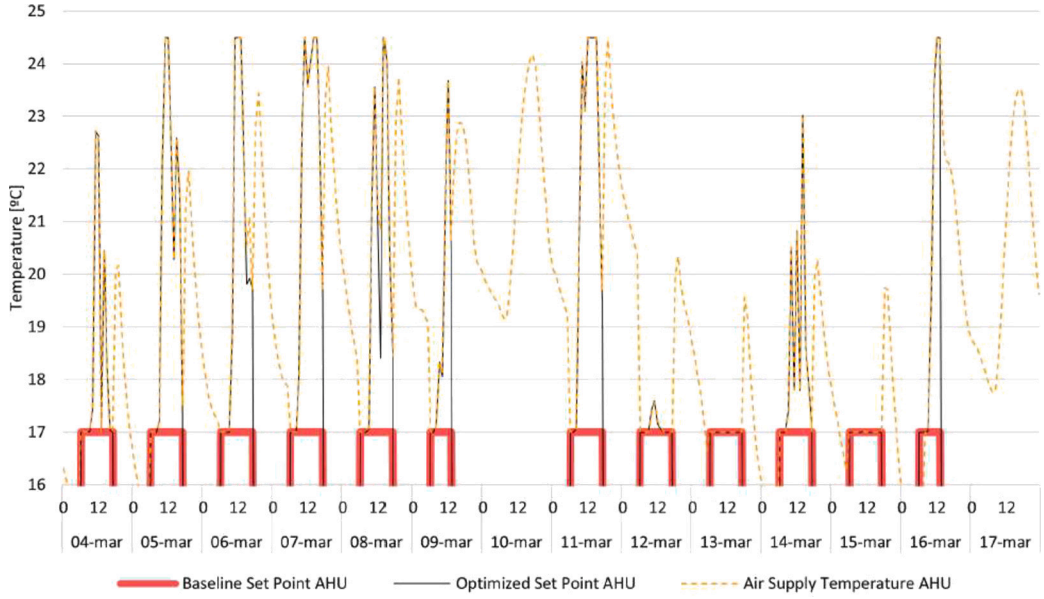

Fig. 14. AHU Supply Air Temperature Set-Point comparison between baseline and optimization for March (winter scenario).

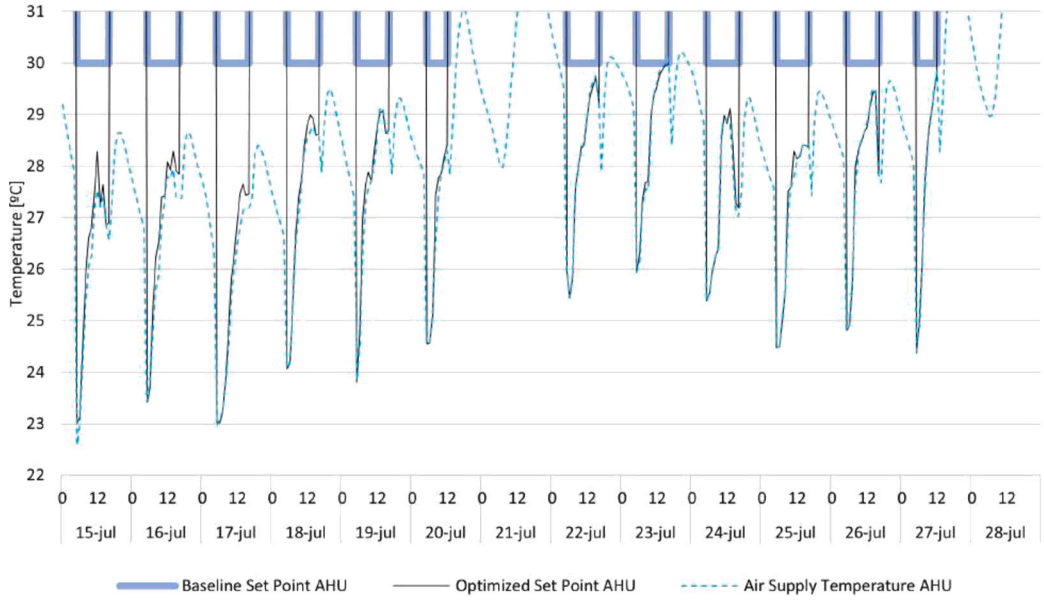

Fig. 15. AHU Supply Air Temperature Set-Point comparison between baseline and optimization for August (summer scenario).

Funding

The researchers Carlos Fernández Bandera, Jose Pachano and María Fernández-Vigil Iglesias have been funded by the Government of Navarra under the project “From BIM to BEM: B&B” (ref. 0011-1365-2020-000227).

Abbreviations

The following abbreviations are used in this manuscript:

AHU	Air Handling Unit
ASHRAE	American Society of Heating, Refrigerating and Air-Conditioning Engineers
BEM	Building Energy Model
BMS	Building Management System
CIBSE	Chartered Institution of Building Services Engineers
COP	Coefficient of Performance
Csa	Hot-Summer Mediterranean Climate
Cv(RMSE)	Coefficient of Variation of Mean Square Error
CO_2	Carbon dioxide
DSM	Demand Side Management
DX	Direct Expansion
EEV	Electronic Expansion Valves
EPS	Expanded Polystyrene
Erl	EnergyPlus Runtime Language
EU	European Union
FCU	Fan Coil Unit
HP	Heat Pump
HVAC	Heating, Ventilation and Air Conditioning
$L(t)$	Instantaneous building power consumption
LTCP	Lavrion Technological and Cultural Park
MAE	Mean Absolute Error
MPC	Model Predictive Control
$M(t)$	Instantaneous overlapping of generation and load profile
NMBE	Normalized Mean Bias Error

NTUA	National Technical University of Athens
nZEB	Nearly Zero-Energy Building
NZEB	Net Zero-Energy Building
$P(t)$	Instantaneous on site PV generation
PV	Photovoltaic
R^2	Spearman's Rank Correlation Coefficient Square
RB	Rule Based
RMSE	Root Mean Square Error
SABINA	SmArt BI-directional multi eNergy gAteway
SC	Self-Consumption
SS	Self-Sufficiency
Temp.	Temperature
TZ	Thermal Zone
VRF	Variable Refrigerant Flow
γ_{sc}	Self-Consumption
γ_{ss}	Self-Sufficiency
$\Delta\Theta$	Temperature Differential Range
°C	Celsius degrees
cm	Centimeters
kW	Kilowatt
kWh	Kilowatt per hour
kWp	Kilowatt peak
mm	Millimeters
m^2	Square meters
m/s	Meters per second
m^3/h	Cubic meters per hour
Pa	Pascals
W	Watts
%	Percentage
° or deg	Decimal degrees

CRediT authorship contribution statement

Conceptualization, J.P., M.F.I. and C.F.B.; Methodology, J.P. and C.F.B.; Software, J.P. and M.F.I.; Validation, J.P. and C.F.B.; Investigation, J.P., M.F.I. and C.F.B.; Resources, C.F.B.; Data Provider: A.P.; Writing–original draft preparation, J.P. and M.F.I.; Writing–review and editing, J.P., M.F.I., A.P. and C.F.B.; Supervision, C.F.B.; Project Administration, C.F.B.; Funding Acquisition, C.F.B. All authors have read and agreed to the published version of the manuscript.

Declaration of competing interest

The authors declare that they have no known competing financial interests or personal relationships that could have appeared to influence the work reported in this paper.

Data availability

The authors do not have permission to share data.

Acknowledgements

We would like to thank National Technical University of Athens (Greece), for providing us with both the building documentation and the sensor data to perform the necessary tests for this paper. Data collection was gathered from the European Project "SABINA".

References

[1] European Commission and Directorate-General for Energy, Clean energy for all Europeans, Technical Report, 2019.
[2] European Commission, COM(2020) 562 final: Stepping up Europe's 2030 climate ambition. Investing in a climate-neutral future for the benefit of our people, Technical Report, Brussels, 2020.
[3] European Parliament, Council of the European Union, European green deal: fit for 55, https://www.consilium.europa.eu/en/policies/green-deal/fit-for-55-the-eu-plan-for-a-green-transition/, 2023. (Last access: 19-07-2023).
[4] I. Kougias, N. Taylor, G. Kakoulaki, A. Jäger-Waldau, The role of photovoltaics for the European green deal and the recovery plan, Renew. Sustain. Energy Rev. 144 (2021) 111017, https://doi.org/10.1016/j.rser.2021.111017.
[5] European Parliament, Council of the European Union, Directive 2010/31/eu of the European Parliament and of the council of 19 may 2010 on the energy performance of buildings, http://data.europa.eu/eli/dir/2010/31/oj, 2010. (Last access: 07-12-2022).
[6] European Parliament, Council of the European Union, Directive (EU) 2018/844 of the European Parliament and of the Council of 30 May 2018 amending Directive 2010/31/EU on the energy performance of buildings and Directive 2012/27/EU on energy efficiency, https://eur-lex.europa.eu/legal-content/EN/TXT/HTML/?uri=CELEX:32018L0844, 2018. (Last access: 19-07-2023).
[7] S. Pless, P. Torcellini, Net-zero energy buildings: a classification system based on renewable energy supply options, Technical Report, National Renewable Energy Lab. (NREL), Golden, CO (United States), 2010.
[8] K. Voss, I. Sartori, R. Lollini, Nearly-zero, net zero and plus energy buildings, REHVA J. (Dec 2012) 23–27, https://task40.iea-shc.org/Data/Sites/1/publications/Task40-A-Nearly-zero-Net-zero-and-Plus-Energy-Buildings.pdf, (Last access: 28-08-2023).
[9] Y. Luo, Y. Shi, Y. Zheng, Z. Gan, N. Cai, Strategy for renewable energy storage in a dynamic distributed generation system, Energy Proc. 105 (2017) 4458–4463, https://doi.org/10.1016/j.egypro.2017.03.946.
[10] N.K. Meena, A. Swarnkar, N. Gupta, K.R. Niazi, Optimal accommodation and management of high renewable penetration in distribution systems, J. Eng. 2017 (2017) 1890–1895, https://doi.org/10.1049/joe.2017.0659.
[11] J. Widén, E. Wäckelgård, P.D. Lund, Options for improving the load matching capability of distributed photovoltaics: methodology and application to high-latitude data, Sol. Energy 83 (2009) 1953–1966, https://doi.org/10.1016/j.solener.2009.07.007.
[12] A. Colmenar-Santos, A.-R. Linares-Mena, E.-L. Molina-Ibáñez, E. Rosales-Asensio, D. Borge-Diez, Technical challenges for the optimum penetration of grid-connected photovoltaic systems: Spain as a case study, Renew. Energy 145 (2020) 2296–2305, https://doi.org/10.1016/j.renene.2019.07.118.
[13] J. Widén, Improved photovoltaic self-consumption with appliance scheduling in 200 single-family buildings, Appl. Energy 126 (2014) 199–212, https://doi.org/10.1016/j.apenergy.2014.04.008.
[14] J.M. Roldán Fernández, M. Burgos Payán, J.M. Riquelme Santos, Profitability of household photovoltaic self-consumption in Spain, J. Clean. Prod. 279 (2021) 123439, https://doi.org/10.1016/j.jclepro.2020.123439.
[15] J.M. Roldan-Fernandez, M. Burgos-Payan, J.M. Riquelme-Santos, Assessing the decarbonisation effect of household photovoltaic self-consumption, J. Clean. Prod. 318 (2021) 128501, https://doi.org/10.1016/j.jclepro.2021.128501.
[16] D. Talavera, F. Muñoz-Rodriguez, G. Jimenez-Castillo, C. Rus-Casas, A new approach to sizing the photovoltaic generator in self-consumption systems based on cost–competitiveness, maximizing direct self-consumption, Renew. Energy 130 (2019) 1021–1035, https://doi.org/10.1016/j.renene.2018.06.088.
[17] D. Chiaroni, V. Chiesa, L. Colasanti, F. Cucchiella, I. D'Adamo, F. Frattini, Evaluating solar energy profitability: a focus on the role of self-consumption, Energy Convers. Manag. 88 (2014) 317–331, https://doi.org/10.1016/j.enconman.2014.08.044.
[18] I. Saviuc, H. Peremans, S. Van Passel, K. Milis, Economic performance of using batteries in European residential microgrids under the net-metering scheme, Energies 12 (2019) 165, https://doi.org/10.3390/en12010165.
[19] S.Ø. Jensen, A. Marszal-Pomianowska, R. Lollini, W. Pasut, A. Knotzer, P. Engelmann, A. Stafford, G. Reynders, IEA EBC Annex 67 energy flexible buildings, Energy Build. 155 (2017) 25–34, https://doi.org/10.1016/j.enbuild.2017.08.044.
[20] H. Li, Z. Wang, T. Hong, M.A. Piette, Energy flexibility of residential buildings: a systematic review of characterization and quantification methods and applications, Adv. Appl. Energy 3 (2021) 100054, https://doi.org/10.1016/j.adapen.2021.100054.
[21] T.Q. Péan, J. Salom, R. Costa-Castelló, Review of control strategies for improving the energy flexibility provided by heat pump systems in buildings, J. Process Control 74 (2019) 35–49, https://doi.org/10.1016/j.jprocont.2018.03.006.
[22] A. Chabaud, J. Eynard, S. Grieu, A rule-based strategy to the predictive management of a grid-connected residential building in southern France, Sustain. Cities Soc. 30 (2017) 18–36, https://doi.org/10.1016/j.scs.2016.12.016.
[23] M. Pinamonti, A. Prada, P. Baggio, Rule-based control strategy to increase photovoltaic self-consumption of a modulating heat pump using water storages and building mass activation, Energies 13 (2020) 6282, https://doi.org/10.3390/en13236282.
[24] E. Bee, A. Prada, P. Baggio, Demand-side management of air-source heat pump and photovoltaic systems for heating applications in the Italian context, Environments 5 (2018) 132, https://doi.org/10.3390/environments5120132.
[25] U.I. Dar, I. Sartori, L. Georges, V. Novakovic, Advanced control of heat pumps for improved flexibility of net-zeb towards the grid, Energy Build. 69 (2014) 74–84, https://doi.org/10.1016/j.enbuild.2013.10.019.
[26] L. Schibuola, M. Scarpa, C. Tambani, Demand response management by means of heat pumps controlled via real time pricing, Energy Build. 90 (2015) 15–28, https://doi.org/10.1016/j.enbuild.2014.12.047.
[27] R. De Coninck, R. Baetens, D. Saelens, A. Woyte, L. Helsen, Rule-based demand-side management of domestic hot water production with heat pumps in zero energy neighbourhoods, J. Build. Perform. Simul. 7 (2014) 271–288, https://doi.org/10.1080/19401493.2013.801518.

[28] SABINA H2020 EU program, https://cordis.europa.eu/project/id/731211/es, 2016-2020. (Accessed 21 February 2023).
[29] SmArt BI-directional multi eNergy gAteway: SABINA project, https://sabina-project.eu/, 2016-2020. (Accessed 20 July 2023).
[30] G. Ramos Ruiz, C. Fernandez Bandera, Validation of calibrated energy models: common errors, Energies 10 (2017) 1587, https://doi.org/10.3390/en10101587.
[31] G. Ramos Ruiz, C. Fernández Bandera, Analysis of uncertainty indices used for building envelope calibration, Appl. Energy 185 (2017) 82–94, https://doi.org/10.1016/j.apenergy.2016.10.054.
[32] G. Ramos Ruiz, E. Lucas Segarra, C. Fernández Bandera, et al., Model predictive control optimization via genetic algorithm using a detailed building energy model, Energies 12 (2018) 1–18, https://doi.org/10.3390/en12010034.
[33] G.R. Ruiz, C.F. Bandera, T.G.-A. Temes, A.S.-O. Gutierrez, Genetic algorithm for building envelope calibration, Appl. Energy 168 (2016) 691–705, https://doi.org/10.1016/j.apenergy.2016.01.075.
[34] C. Fernández Bandera, G. Ramos Ruiz, Towards a new generation of building envelope calibration, Energies 10 (2017) 2102, https://doi.org/10.3390/en10122102.
[35] J.E. Pachano, C. Fernández Bandera, Multi-step building energy model calibration process based on measured data, Energy Build. 252 (2021) 111380, https://doi.org/10.1016/j.enbuild.2021.111380.
[36] J.E. Pachano, A. Peppas, C. Fernández Bandera, Seasonal adaptation of vrf hvac model calibration process to a Mediterranean climate, Energy Build. 261 (2022) 111941, https://doi.org/10.1016/j.enbuild.2022.111941.
[37] C. Fernández Bandera, G. Bastos Porsani, M. Fernández-Vigil Iglesias, A demand side management approach to increase self-consumption in buildings, Build. Simul. 16 (2022) 317–335, https://doi.org/10.1007/s12273-022-0933-9.
[38] M. Casini, Chapter 10 - building automation systems, in: Construction 4.0: Advanced Technology, Tools and Materials for the Digital Transformation of the Construction Industry, in: Woodhead Publishing Series in Civil and Structural Engineering, Woodhead Publishing, 2022, pp. 525–581.
[39] C. Beck, J. Grieser, M. Kottek, F. Rubel, B. Rudolf, Characterizing global climate change by means of Köppen climate classification, Technical Report, Deutscher Wetterdienst, Offenbach, Germany, 2005.
[40] E. Lucas Segarra, G. Ramos Ruiz, C. Fernández Bandera, Probabilistic load forecasting for building energy models, Sensors 20 (2020) 6525, https://doi.org/10.3390/s20226525.
[41] E. Lucas Segarra, H. Du, G. Ramos Ruiz, C. Fernández Bandera, Methodology for the quantification of the impact of weather forecasts in predictive simulation models, Energies 12 (2019) 1309, https://doi.org/10.3390/en12071309.
[42] E. Lucas Segarra, G. Ramos Ruiz, V. Gutiérrez González, A. Peppas, C. Fernández Bandera, Impact assessment for building energy models using observed vs. third-party weather data sets, Sustainability 12 (2020) 6788, https://doi.org/10.3390/su12176788.
[43] T.N. Aynur, Variable refrigerant flow systems: a review, Energy Build. 42 (2010) 1106–1112, https://doi.org/10.1016/j.enbuild.2010.01.024.
[44] J.E. Pachano, M. Fernández-Vigil Iglesias, J.C. Saiz, C. Fernández Bandera, Two-stage multi-step energy model calibration of the cooling systems of a large-space commercial building, Appl. Therm. Eng. 230 (2023) 120638.
[45] V. Gutiérrez González, G. Ramos Ruiz, C. Fernández Bandera, Empirical and comparative validation for a building energy model calibration methodology, Sensors 20 (2020) 5003, https://doi.org/10.3390/s20175003.
[46] IPMVP Committee, et al., International Performance Measurement and Verification Protocol: Concepts and options for determining energy and water savings, Volume I, Technical Report, National Renewable Energy Lab., Golden, CO (US), 2001, https://www.nrel.gov/docs/fy02osti/31505.pdf. (Last access: 20-07-2023).
[47] R. Luthander, A.M. Nilsson, J. Widén, M. Åberg, Graphical analysis of photovoltaic generation and load matching in buildings: a novel way of studying self-consumption and self-sufficiency, Appl. Energy 250 (2019) 748–759, https://doi.org/10.1016/j.apenergy.2019.05.058.